JOURNAL OF GEOPHYSICAL RESEARCH: SPACE PHYSICS, VOL. 118, 2087–2100, doi:10.1002/jgra.50248, 2013

Study of small-scale plasmoid structures in the magnetotail using Cluster observations and Hall MHD simulations

Chaoxu Liu,[1] Xueshang Feng,[1] Jianpeng Guo,[1] and Yudong Ye[1,2]

Received 6 September 2012; revised 31 January 2013; accepted 10 March 2013; published 20 May 2013.

[1] The existence of small-scale plasmoids associated with the Hall effect has been often observed in the magnetotail. They are considered as the signature of multiple X-line collisionless reconnection. To study these plasmoids structures, we present some Cluster observations and Hall MHD simulations of their features. In this study, the observation survey is divided into two types. The first one is the isolated plasmoid with two typical plasmoid events the flux-rope-like plasmoid on 3 August 2001 and the closed-loop-like plasmoid on 22 August 2001. The second type contains multiple successive plasmoids, on 12 September 2001 with three neighboring plasmoids structures observed during a substorm. Especially for the second plasmoid, three main features were observed, including a core field in the plasmoid, a quadrupole magnetic field near the X line, and a local plasma convection within the plasmoid. The Grad-Shafranov reconstruction method was used to recover the two-dimensional magnetic field maps for this plasmoid. These results may provide evidence that the small-scale plasmoids frequently observed in the magnetotail may be produced by multiple X-line collisionless reconnection. To study the impact of crosstail magnetic field on the structures of small-scale plasmoids, a 2.5-D Hall MHD simulation was performed. In the case with a guide field B_{y0}, the in-plane plasma inflows carrying B_y flux enter into the plasmoid due to magnetic reconnection. However, there is no such B_y flux transport process for the case without guide field. These results demonstrate that a crosstail magnetic field is an important factor in the formation of flux-rope-like plasmoids.

Citation: Liu, C., X. Feng, J. Guo, and Y. Ye (2013), Study of small-scale plasmoid structures in the magnetotail using Cluster observations and Hall MHD simulations, *J. Geophys. Res. Space Physics*, *118*, 2087–2100, doi:10.1002/jgra.50248.

1. Introduction

[2] The near-Earth neutral line model [*Hones et al.*, 1976] had predicted the existence and kinetic properties of tailward-travelling plasmoids associated with substorms. Large-scale plasmoids in the magnetotail have been observed and studied extensively [*Hones et al.*, 1984; *Moldwin and Hughes*, 1991, 1993; *Slavin et al.*, 1995, 2003a; *Ieda et al.*, 1998]. With the frequent passes through the magnetotail region of satellites such as Cluster, Geotail, and Double Star, small spatial scale plasmoids of $\sim$ 1 Earth radii (R_E) have been observed and investigated in the Earth's magnetotail [*Elphic et al.*, 1986; *Zong et al.*, 1997, 2004; *Ieda et al.*, 1998; *Slavin et al.*, 2003a, 2003b; *Deng et al.*, 2004; *Ohtani et al.*, 2004; *Eastwood et al.*, 2005, 2007; *Walsh et al.*, 2007]. The signatures of magnetic fields inside the plasmoid, which are often observed in the magnetotail, show not only a bipolar variation in the B_z component with an O-shaped magnetic field lines, but display a very large core magnetic field with its amplitude even larger than the lobe magnetic field in some cases. Usually, the direction of the core field is consistent with the direction of the interplanetary magnetic field (IMF) B_y-component [*Moldwin and Hughes*, 1992]. Such plasmoids with a large core B_y field are well-known as "magnetic flux ropes" (MFR) [*Sibeck et al.*, 1984; *Elphic et al.*, 1986; *Hughes and Sibeck*, 1987; *Slavin et al.*, 1989; *Moldwin and Hughes*, 1991; *Ieda et al.*, 1998; *Slavin et al.*, 2003a; *Henderson et al.*, 2006; *Hasegawa et al.*, 2007; *Chen et al.*, 2007]. Besides, observations also indicate the presence of the other kind of plasmoid structures with the waveform (bipolar or multiple bipolar) signatures in B_y and bipolar signatures in B_z. Note that the waveform B_y signatures are observed together with bipolar B_z signatures. This type of structure with closed-loop magnetic field lines, here called closed-loop-like plasmoid, has been observed by many satellites [*Moldwin and Hughes*, 1992; *Zong et al.*, 1997; *Deng et al.*, 2004]. In the present study, the term plasmoid is used for consistent representation of MFR-like and closed-loop-like plasmoid.

[1]SIGMA Weather Group, State Key Laboratory of Space Weather, Center for Space Science and Applied Research, Chinese Academy of Sciences, Beijing, China.

[2]Graduate School, Chinese Academy of Sciences, Beijing, China.

Corresponding author: X. S. Feng, C. X. Liu, SIGMA Weather Group, State Key Laboratory of Space Weather, Center for Space Science and Applied Research, Chinese Academy of Sciences, No. 1 Nanertiao, Zhongguancun, Haidian District, Beijing 100190, China. (fengx@spaceweather.ac.cn, cxliu@spaceweather.ac.cn)

2169-9380/13/10.1002/jgra.50248

[3] The formation of small-scale plasmoids in the magnetotail can be most easily understood in terms of the multiple X-line reconnection (MXR). This model has been used to explain the helical magnetic structure in flux transfer events (FTEs) at the dayside magnetopause during intervals of southward interplanetary magnetic field (IMF) [*Lee et al.*, 1985]. In MXR, each plasmoid is bounded by two adjacent reconnection X lines. The rate of reconnection need not be the same for the two adjacent X line at both sides of the newly formed plasmoid [*Schindler*, 1974]. Once one X-point will reconnect closed field lines in plasma sheet and then open lobe field lines faster than others, the plasmoid may become dynamically unstable. The fastest X-line plays a dominant role, leading to the fast Alfvénic plasma jets carrying wrapped plasmoids that will move away from this X-line. These have been numerically studied extensively [*Ohtani et al.*, 2004; *Drake et al.*, 2006; *Daughton et al.*, 2006; *Liu et al.*, 2011]. *Deng et al.* [2004] provided evidence of multiple X line collisionless reconnection in an active reconnection diffusion region in the Earth's magnetotail on the basis of the following observed features: quadrupole pattern of the out-of-plane B_y component during the passage of a magnetic island, a direction reversal of the electron beams and plasma flow reversal. *Eastwood et al.* [2005] have examined an earthward moving flux rope bounded by two active reconnection sites observed by Cluster spacecraft on 2 October 2003. The results indicated that MXR in the magnetotail current sheet can occur simultaneously, providing experimental validation of mesoscale plasmoid with respect to the MXR theories.

[4] As discussed earlier by *Fairfield* [1979], *Lui* [1984], and *Hughes and Sibeck* [1987], a crosstail magnetic field could be well correlated with the IMF B_y. *Fairfield* [1979] found that the B_y component of IMF penetrates partially ($\sim$ 0.13) into the magnetotail. *Lui* [1984] suggested that about 50% of the IMF B_y component exists in the neutral sheet region. The direction of the core field in MFR is usually along the direction of the B_y component of the IMF [*Hughes and Sibeck*, 1987; *Moldwin and Hughes*, 1992; *Slavin et al.*, 2003a]. In this scenario, a flux-rope-like plasmoid should be considered as a three-dimensional structure. Already, there are many explanations for the generation of the large core field of plasmoid. *Ma et al.* [1994] proposed that the increase in the core magnetic field depends on both the property of the initial configuration and the particular reconnection geometry. *Walker and Ogino* [1996] found that the MFR structure can be formed if there exists an IMF $B_y \neq 0$ in the plasma sheet by using a 3-D global MHD simulation. *Karimabadi et al.* [1999] carried out 2-D and 3-D hybrid simulations, suggesting that the large observed core field in the plasmoid was explained in terms of Hall-generated currents.

[5] The Hall effect is the production of a voltage difference across an electrical conductor in which an electric current flows in a magnetic field. The direction of the voltage difference is perpendicular to both the magnetic field and the current. It was discovered by *Hall* [1879] and had been verified experimentally in many different scenarios, such as the experiment for the Hall effect during magnetic reconnection in a laboratory plasma [*Ren et al.*, 2005]. Hall effect also plays an important role in collisionless magnetic reconnection [*Wang et al.*, 2001], which can give rise to the decoupling of ions from electrons. The dissipation region develops a multiscale structure [*Sonnerup*, 1979; *Biskamp et al.*, 1997; *Shay et al.*, 1998; *Birn et al.*, 2001]. Below the ion inertial length d_i ($d_i \equiv c/\omega_{pi}$, where ω_{pi} is the ion plasma frequency), the Hall currents can produce a quadrupolar out-of-plane magnetic field [*Terasawa*, 1983], which can be as a key feature of collisionless reconnection. Such signatures has been observed by a number of satellites [*Deng and Matsumoto*, 2001; *Øieroset et al.*, 2001; *Vaivads et al.*, 2004; *Borg et al.*, 2005]. The magnetotail current sheet becomes thinner during the substorm growth phase [*Kaufmann*, 1987; *Lui et al.*, 1992]. The multiple X-line reconnection in the thin current sheet can occur due to the tearing-mode instability. When the thickness of the current sheet is shorter than or equal to the ion-inertial length scale [*Sonnerup*, 1979] during the current sheet thinning, one needs to take into consideration the influence of the Hall effect on the structure of plasmoids. There are plentiful of observational evidences for the Hall effect. *Eastwood et al.* [2007] found a mirror image Hall field structure around the diffusion region by using multipoint Cluster observation. The average properties of the magnetic reconnection ion diffusion region in the Earth's magnetotail have been investigated by *Eastwood et al.* [2010], in which the average peak Hall magnetic field was 0.39 ± 0.16, the average peak Hall electric field was 0.33 ± 0.18, and the average out-of-plane electric field was ~ 0.04. *Wang et al.* [2010] reported a secondary magnetic island in an ion diffusion region observed by Cluster. Enhancement of the energetic electron fluxes and a large core magnetic field inside the secondary island were observed at the same time. The Hall electric field E_N pointed to the center of the neutral sheet, and the out-of-plane magnetic field B_M was also detected [*Wang et al.*, 2010]. These observations indicate that the Hall effect in reconnection cannot be ignored in the analysis of plasmoid formation process in the magnetotail.

[6] We had investigated the structures of plasmoid-like using Hall MHD [*Liu et al.*, 2009]. The results indicate that: (1) Hall effect and a preexisting crosstail component B_y are two important factors controlling the occurrence of various plasmoid-like structures in the magnetotail; and (2) the interaction between Hall effect and the added-B_y flux constitutes the most important contribution to the growth of the core field in plasmoid [*Liu et al.*, 2009]. In addition, we carried out 2.5-D Hall MHD simulations to study the evolution of moving-plasmoid [*Liu et al.*, 2011], in which the features of the Hall fields can be consistent with the observations [*Deng et al.*, 2004; *Eastwood et al.*, 2007]. In the present work, we use the Cluster observations combined with the Grad-Shafranov (GS) reconstruction and Hall MHD simulation to study the structural features of small-scale plasmoids in the magnetotail. Several typical observations have been analyzed for both single and multiple plasmoids under different environmental conditions. Especially for the plasmoid on 12 September 2001, three main features were observed, including a large core field B_y in the plasmoid, a quadrupole magnetic field near the X line, and a local plasma convection within the plasmoid. The GS reconstruction method was used to reproduce two-dimensional magnetic field maps for this plasmoid. The results show that a flux-rope-like plasmoid was moving tailward, and its diameter was about $1R_E$ in the x-direction. To study the impact of crosstail

magnetic field on the structures of small-scale plasmoids, a 2.5-D Hall MHD simulation was performed. The signatures of magnetic field components inside the plasmoids obtained from the simulations are in qualitative agreement with the Cluster observations.

[7] The organization of this paper is as follows. In section 2, we analyze the observational features for several typical plasmoid events. The simulation results of two cases with and without guide field, which focus on the interpretation and comparison with the observations made by Cluster spacecraft, are presented in section 3. The basic results are summarized in section 4, and a discussion is made about the specific causes of the observed features.

2. Observations and Analysis

[8] The analyzed observations in this section were made by the Cluster spacecraft in the magnetotail during the three intervals of interest: 11:05–11:15 UT on 3 August 2001, 09:46–09:52 UT on 22 August 2001, and 13:13:00–13:18:00 UT on 12 September 2001. The first two intervals above include the most prominent properties of plasmoid, while the last one has three neighboring plasmoids during a geomagnetic substorm. These events were analyzed using the plasma data and magnetic field from the flux gate magnetometer (FGM) [*Balogh et al.*, 2001] and the Cluster ion spectrometry (CIS) [*Rème et al.*, 2001] instruments. The 16 s averaged IMF data for each interval of these events were obtained by the ACE Magnetic Field Instrument (MAG) [*Smith et al.*, 1998]. Below, we detail these examples that help to understand the properties of small-scale plasmoids before giving the simulation results.

2.1. Single Plasmoid Observations

[9] An example of an earthward-moving plasmoid event with a large core B_y field is presented in Figures1b–1e at 4 s resolution in Geocentric Solar Magnetospheric (GSM) coordinates. This plasmoid was observed by Cluster spacecraft between 11:08:40 and 11:09:48 UT on 3 August 2001. The centroid of the four Cluster spacecraft was located at (–16.8, –8.5, and 2.1) R_E in GSM coordinates. A south-then-north reversal of B_z marked by dashed vertical line in Figure 1d is shown at 11:09:30 UT. The primary signatures in this plasmoid, including the strong core field B_y, the bipolar (negative to positive) variation in B_z, and the near-zero B_x, indicate the plasmoid earthward. The trailing region of the plasmoid was embedded in fast flow (Figure 1e). Shortly thereafter, a bursty bulk flow (BBF) with peak speed up to 900 km/s was observed. The average relative distances between satellites in *xyz*-axes direction are 901.6 km, 999.1 km, and 1030.2 km, respectively. Here, assume that the magnetic structure is stationary and the plasmoid is moving at constant velocity (V_0) along the *x*-direction. The timing of Cluster 4 gives $V_0 \approx 221$ km/s. Based on the bipolar B_z signature, the duration of plasmoid crossing 11:08:40–11:09:48 UT is $\sim$ 68 s, which corresponds to a plasmoid diameter in the *x*-direction of about $\sim 2.4R_E$. The IMF conditions are presented in Figure 1a. The three components of the IMF data for the interval 10:09–11:09 UT on 3 August 2001 were measured by ACE spacecraft at the L1 Lagrangian point. The intensity and polarity of B_x, B_y, and B_z, show that the IMF was dominated by a negative B_y and predominantly

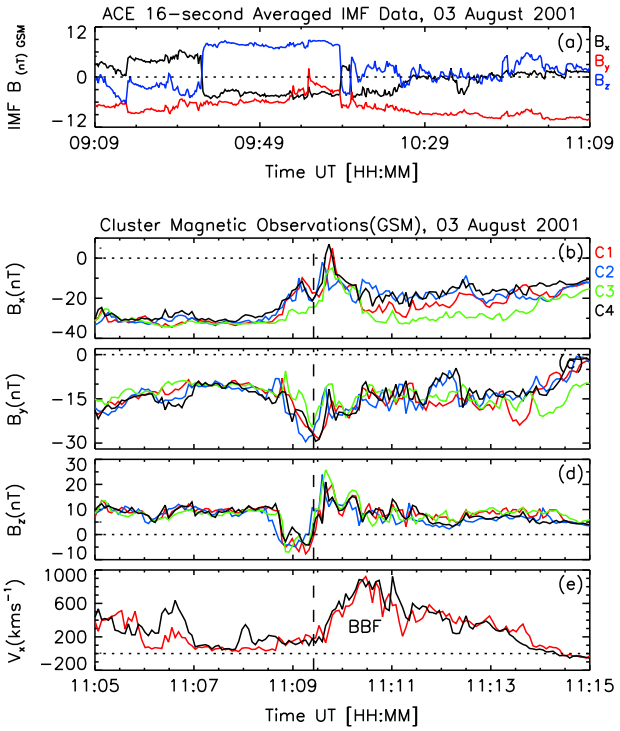

Figure 1. Top panel shows ACE 16 s averaged IMF data: B_x, B_y and B_z in GSM coordinates on 3 August 2001 between 10:09-11:09 UT. The bottom four panels display Cluster magnetic field and plasma data for 3 August 2001, 11:05-11:15 UT. V_x are shown only for Cluster spacecraft 1 and 4. The reversal of B_z is denoted by the vertical black dashed lines.

southward for this interval. During the passage of the plasmoid, an enhanced core magnetic field was recorded, peaking at nearly 30.4 nT (Figure 1c). Considering the IMF conditions for several hours preceding the observations of this plasmoid, the continued presence of large B_y-dominated IMF in the plasma sheet might have caused the formation of very strong core magnetic field in plasmoid as explained by *Cowley* [1981].

[10] Another example of a plasmoid encountered by Cluster spacecraft between 09:46:00 UT and 09:52:00 UT on 22 August 2001, is presented in Figure 2. The centroid of the four Cluster spacecraft was located at (–18.9, –3.3, and 1.0) R_E in GSM coordinates at 09:50 UT. The data analyzed here have been investigated by *Eastwood et al.* [2007]. Figure 2a shows the three components of the IMF measured by ACE during the 2 h intervals (07:50–09:50 UT) prior to the plasmoid. This plasmoid had magnetic field signatures and its associated IMF conditions slightly different from the previous one. Here, we calculate the mean values of the IMF components during this period, in order to determine the interplanetary magnetic field conditions during the formation of the plasmoid. The mean value of the IMF B_y was –1.21 nT smaller than the previous plasmoid event with a mean value of $\sim$ –7.25 nT. Accordingly, the small cross-tail component $|B_y|$ in the magnetotail is likely due to the small IMF B_y mapped into the magnetotail

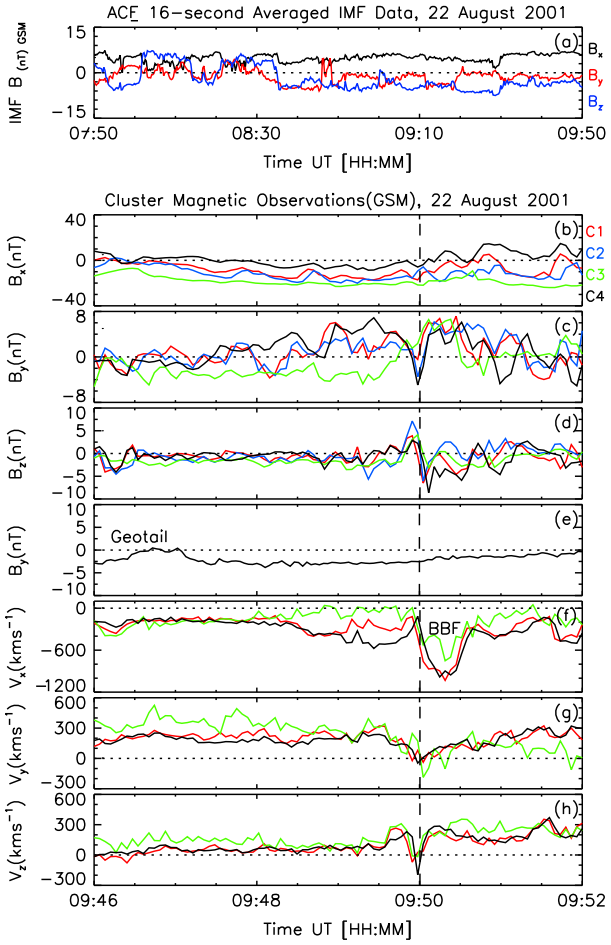

Figure 2. Top panel shows ACE 16 s averaged IMF data: B_x, B_y and B_z in GSM coordinates on 22 August 2001 between 08:50-09:50 UT. Panel (e) displays B_y observed by Geotail. Panels (b)-(d) display B_x, B_y and B_z, and Panels (f)-(h) are the *xyz* components of the ion velocity in GSM coordinates, measured by the Cluster spacecraft 1, 3, and 4 on 22 August 2001 between 09:46-09:52 UT. The reversal of B_z is denoted by the vertical black dashed lines.

[*Cowley*, 1981]. As shown in Figure 2e, B_y outside the magnetosphere, which was recorded by Geotail spacecraft, is small compared to that in the magnetotail. From these considerations, the magnetic field does not include a significant guide field during the formation of plasmoid. All satellites were located below the current sheet ($B_x < 0$). Cluster 4 was closest to the current sheet and the other satellites were located below it during this interval. The north-to-south reversal of B_z is marked by the dashed vertical line just after 09:50 UT (see Figure 2d). Correspondingly, an obvious BBF-type jetting plasma was observed. The bipolar variation of B_z accompanied by tailward flow shows that a tailward-travelling of plasmoid passed through satellites [*Slavin et al.*, 2003a]. Here, compared to the previous case, there is a waveform variation in B_y coincident with the $\pm B_z$ reversal (see Figures 2c and 2d). The B_y history recorded by Cluster 4 is first positive then negative and finally turns into a positive. The B_y changes from negative to positive for Cluster 3. As shown in Figure 2g, the magnitude of $|V_y|$ recorded by Cluster spacecrafts 1, 2, and 3 are close to zero in the central region of the plasmoid, while this value increases gradually away from the center as observed by Cluster spacecrafts 1 and 4. It is V-shaped. At the same time, the bipolar signature (+/–) of V_y was observed by Cluster 3. In Figure 2h, the V_z close to zero inside the plasmoid, but are two pulse shapes outside the plasmoid. It is M-shaped.

[11] In the examples described above, we present two typical Cluster observations of earthward/tailward-moving plasmoids in the tail. For the plasmoid during 11:08:40–11:09:48 UT on 3 August 2001, its main features are: (1) The B_z show a south-then-north bipolar variation, followed by local high-speed plasma flows within several minutes. (2) The B_y field enhancement occurs during field reversal in B_z. (3) The value of $|B_x|$ is close to zero when the Cluster spacecraft passes through the center of plasmoid. These generic features are often served as the observational signatures of flux rope structures, which was also called BBF-like flux rope by *Slavin et al.* [2003a]. The other one is a tailward plasmoid with a northward-to-southward B_z bipolar magnetic signature encountered by Cluster spacecraft from 09:49:44 UT to 09:50:08 UT on 22 August 2001. Correspondingly, such plasmoid was called plasmoid-like flux rope [*Slavin et al.*, 2003a]. Interestingly, during the encounter, a bipolar waveform signature in B_y component accompanied by the bipolar signatures of B_z is present. Generally speaking, the earthward plasmoids with a southward-to-northward B_z signature and tailward plasmoids with north-then-south B_z signature, often being inlaid in a high-speed stream [*Slavin et al.*, 2003a], are most easily understood according to the MXR model [*Lee et al.*, 1985]. During the substorm growth phase, the thin current sheet in the magnetotail becomes unstable, leading to the formation of multiple plasmoids [*Liu et al.*, 2009]. In addition, observations of plasmoids are highly correlated with substorm signatures [*Moldwin and Hughes*, 1993; *Nagai et al.*, 1994]. In the next section, we will present in detail the observation of multiple plasmoids associated with the Hall effect during a substorm for the first time.

2.2. Multiple Plasmoids Observation

[12] On 12 September 2001, multiple plasmoids were observed during the course of the substorm. The centroid of the four Cluster spacecraft was located at (–18.8, 3.1, and 1.4) R_E in GSM coordinates when the substorm started at ~13:00 UT. Figure 3 shows a summary of Cluster observations for the interval from 13:13:00 to 13:18:00 UT on 12 September 2001. Figures 3a–3d display the magnetic field components B_x, B_y, and B_z and the total magnetic field B at 0.045 s resolution in GSM coordinates. Subsequent three panels show the plasma parameters: ion velocity component V_x in GSM coordinates, ion density (n_i), and temperature (T_i) plotted at the time resolution of 4.021 s. Here, for convenience, we name the neighboring plasmoids marked with three vertical dashed lines as plasmoid-1, plasmoid-2, and plasmoid-3, which are identified by the south-then-north reversals of B_z.

[13] The top panel of Figure 3 shows $B_x > 0$ during intervals of plasmoids, indicating that all four Cluster spacecrafts were, at the time, in the northern lobe of the magnetotail. Cluster spacecraft each first encountered an earthward

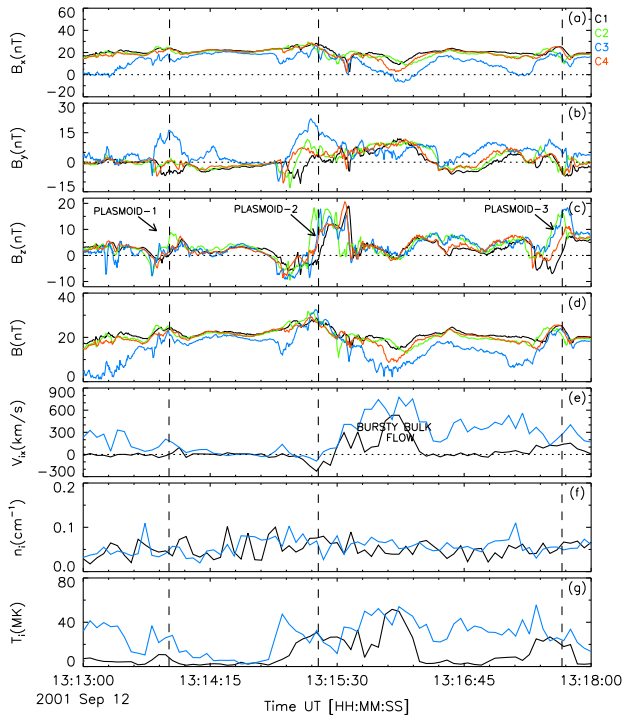

Figure 3. Cluster observation of three successive plasmoids during the interval 13:13–13:18 UT on 12 September 2001. Panels a–d show B_x, B_y and B_z and the total magnetic field B. Panels e–g show ion velocity component (V_{ix}), ion density (n_i), ion temperature (T_i), measured by the Cluster spacecraft 1 and 3 in the GSM coordinates. Three vertical dashed lines denote plasmoid-1, 2, and 3 observed by Cluster 1.

plasmoid (plasmoid-1) during the period of 13:13:39 UT to 13:14:02 UT. As shown in Figure 3c, plasmoid-1 first observed by Cluster 3 (blue line) can be identified by the bipolar B_z signature changing from –12 nT to 10 nT. The peak-to-peak amplitude (δB_z) of B_z are 9 nT, 17.5 nT, 22 nT, and 14 nT for Cluster 1-4. Obviously, the value of δB_z recorded by Cluster 3 is larger than those observed by adjacent Cluster spacecrafts 1, 2, and 4. In addition, the time interval of plasmoid, corresponding to Cluster 3, is longer than others. These differences may be related to the different path of four satellites crossing plasmoid-1. Cluster 3 was located initially in the neutral sheet identified by the $B_x \sim 0$ (see Figure 3a) before plasmoid-1 encountering. It then gradually moved into the north lobe indicated by the moderate increase of B_x toward positive value and the change of temperature. In the center region of plasmoid-1 at about 13:13:42 UT, Cluster 3 observed the positive value of the B_y component and the enhancement of the ion temperature T_i. In addition, a compression of the plasma density is ahead of plasmoid-1 [*Slavin et al.*, 2003a]. Cluster spacecrafts 1, 2, and 4 were in the north-lobe indicated by $B_x > 0$ during the same period. There are no apparent enhancements in plasma density and ion temperature recorded by Cluster 1. Particularly interesting is that the Cluster spacecrafts 1, 2, and 4 recorded a negative value of B_y compared with a positive value of B_y recorded by Cluster 3. The main causes of positive/negative B_y within plasmoid-1 might be related to the Hall effect in collisionless plasma.

[14] A second tailward-moving plasmoid (plasmoid-2) was observed during the period of 13:14:47 UT to 13:15:38 UT. Here, we will analyze in detail this event, in which a clear bipolar B_z variation was observed by Clusters 2 and 4 at 13:15:04 UT, followed by Cluster 3 just after $\sim$ 2 s later, and then by Cluster 1 at 13:15:18 UT. Of particular interest is the observation of B_y during the Cluster spacecraft passage through plasmoid-2 (Figure 3b). Plasmoid-2 observed by Cluster 3 exhibits not only the usual bipolar signature in B_z, but a very large core field B_y (whose peak intensity $\sim$ 22.6 nT can approach the ambient lobe magnetic field). However, multiple bipolar B_y signatures, which may be related to the Hall effect associated with the two neighboring X lines, were observed by the Cluster spacecrafts 1, 2, and 4.

[15] In Figure 3e, ahead of plasmoid-2, the x-component of flow velocity is about of –200 km/s. An earthward bursty bulk flow with a peak velocity $\sim$ 800 km/s, within approximately 1 min after plasmoid-2, has been observed by the Cluster spacecrafts 1 and 3. By comparing the average velocity of bulk flow obtained by the Cluster spacecrafts 1 and 3, Cluster 3 has a higher speed. Such observations may be related to the Cluster 3 spacecraft located closest to the neutral sheet (identified by the minimum B_x and B shown in Figures 3a and 3d). Figure 3g presents plots of the ion temperature measured by CIS ion instruments [*Rème et al.*, 2001] onboard both the Cluster spacecrafts 1 and 3. The existence of high ion temperature in plasmoid-2 may originate from magnetic reconnection occurring simultaneously on both reconnection sites of plasmoid-2. During the interval 13:17:33-13:17:50 UT, the third plasmoid (plasmoid-3) was observed shortly after the two successive plasmoids (plasmoid-1 and plasmoid-2) have been observed. Cluster 1 and Cluster 4 passed through the body of plasmoid-3 (identified by the B_z's sign from negative toward positive), while at the same time, the other two Cluster spacecraft might be located within the traveling compression regions produced by plasmoid-3 (see Figure 3c).

[16] Figures 4a–4d show the magnetic field component B_z and the plasma velocity components V_{ix}, V_{iy}, and V_{iz} in GSM coordinates. We show data from Cluster 1 (black line) and Cluster 3 (blue line) only. The reversal in B_z recorded by Cluster 1 are marked by a vertical dashed line. In Figure 4c, the magnitude of $|V_{iy}|$ recorded by Cluster 1 is close to zero in the central region of plasmoid-2, while this value increases gradually away from the center. It is an inverted V-shape. In Figure 4d, near the center of plasmoid-2, V_{iz} shows (+/–) bipolar signature, which may indicate the presence of plasma convection in the z-direction of plasmoid-2. These observations can also be found in plasmoid-3. In order to explore these flow structures, using the simulation results of Case 1, a cut line have been done at $z_1 = 1.1d_i$ along the x direction as shown in Figure 4e by solid line. The z component of the magnetic field and the xyz components of the ion velocity along this cut line are plotted in Figure 4f. B_z, V_{ix}, V_{iy}, and V_{iz} are expressed by black, gray, blue, and red lines, respectively. In the center region of the plasmoid about $x = 33.3d_i$, the direction of V_{iz} has changed from negative to positive, implying there exist reversed ion flows therein. In Figure 4e, overlooking the entire flow velocity

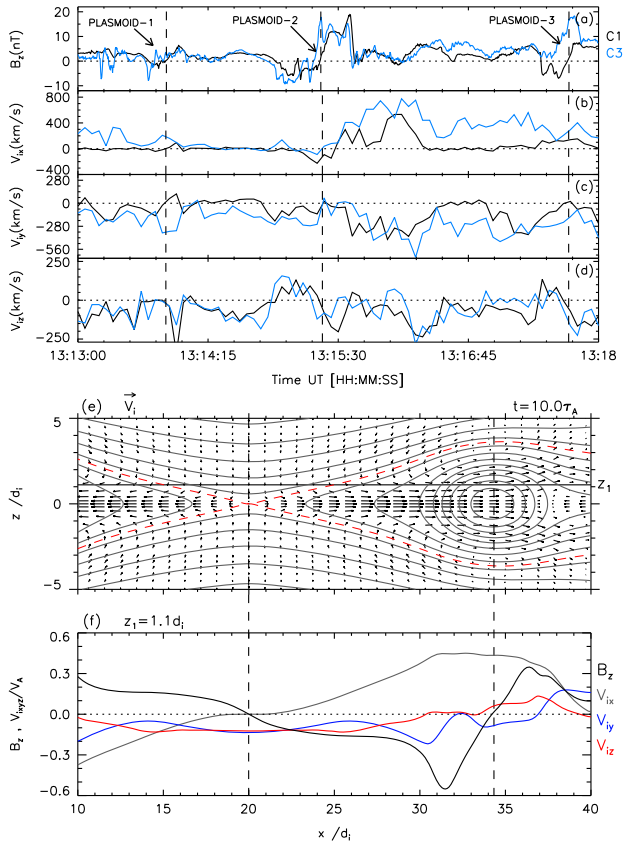

Figure 4. Panels a–d show B_z, V_{ix}, V_{iy} and V_{iz} measured by the Cluster spacecraft 1 and 3 in the GSM coordinates during the interval 13:13-13:18 UT on 12 September 2001. Panel e shows the magnetic field line (solid line), the velocity vector of the plasma flow (arrows), and the magnetic separatrices (red dashed line) for Case 1 at $t = 10.0\tau_A$. B_z, V_{ix}, V_{iy}, and V_{iz} along the cut line are plotted in panel f. The vertical dashed lines denote the B_z-reversal points.

vector within the plasmoid, we can find the bipolar signature in V_{iz} shown in Figure 4f is associated to the vortex of velocity field. To better illustrate the vortex structures in the plasmoid, a numerical simulation (called Case 3) has been carried out. In Case 3, the plasmoid is flanked by two X points with the same reconnection rate. The distribution of the ion velocity V_i at $t = 19.5\tau_A$ is shown in Figure 5a. V_i and magnetic separatrices are expressed by the black arrows and red dashed line, respectively. In Figure 5a, there are four symmetric vortexes in the plasmoid. As Figure 4e, a cut line has also been done at $z_2 = 1.1d_i$ along the x direction shown in Figure 5a by solid line. The z component of the magnetic field and the xyz components of the ion velocity along this cut line are plotted in Figure 5b. B_z, V_{ix}, V_{iy}, and V_{iz} are expressed by black, gray, blue, and red lines, respectively. The profile of V_{iz} (red line) shows two symmetric bipolar variations associated with the vortexes. Comparing Figure 4e with Figure 5a, the distribution of the structure of vortex flow in the plasmoid is different. In Figure 4e, the vortexes located on the same side of the fastest X line have achieved a dominated position. Accordingly, as seen in Figure 4f (red line), the location of the reversal point of V_{iz} near the fastest X line has also moved toward the center of the plasmoid. Comparing the observations with the simulation results, the counter-streaming distributions in plasmoid-2 may indicate the existence of two active reconnection sites. Generally speaking, the plasmoids with a flux rope core were often observed about the leading edge of the bursty bulk flows, such a feature has been investigated by *Slavin et al.* [2003a]. These high-speed earthward bursty bulk flows typically changes from several hundred km/s to exceed 2000 km/s [*Angelopoulos et al.*, 1992; *Slavin et al.*, 2003a], which could weaken the observation frequency of the convection signatures within plasmoid.

[17] The estimated size of each plasmoid is made by $|V_P|$*dt, where $|V_p|$ is the average plasma velocity within plasmoid, dt is the time spent for the plasmoid passing through the satellites. In Figure le, we take V_x = 221 km/s as the approximate velocity of the overall plasmoid structure, where V_x is the average plasma velocity within the plasmoid. The time spent for the plasmoid passing through the satellites is of about 70 s. During this period, the B_z field changes its sign (11:08:40–11:09:50 UT). Here, we assume that the satellites move very slowly to the plasmoid. Accordingly, from the above data, the spatial scale of this plasmoid is estimated to be 15,470 km ($\sim 2.4R_E$) in the x-axis direction. Examining Figure 2, using the same method mentioned above, the length (along x-axis) of the tailward-moving plasmoid is about 13,032 km ($\sim 2.0R_E$). The scale lengths of plasmoid-1, 2, and 3 are $\sim 0.4R_E$, $1.0R_E$, and $0.7R_E$, respectively. Compared to observations from Cluster spacecraft, the average size of the plasmoid in the simulations is about $10d_i$ ($\sim 1.1R_E$) (where the $d_i \equiv c/\omega_{pi}$ is the ion inertial length) along x-axis, and $5d_i$ ($\sim 0.6R_E$) along z-axis.

[18] The top panel of Figure 6 shows the AU (black line) and AL (orange line) geomagnetic indices during the time interval 12:00–18:00 UT on 12 September 2001. Plasmoid-2 has been encountered by Cluster spacecraft within roughly a few minutes after the substorm expansion phase onset. Figure 6 (middle left, right) shows the relative spatial

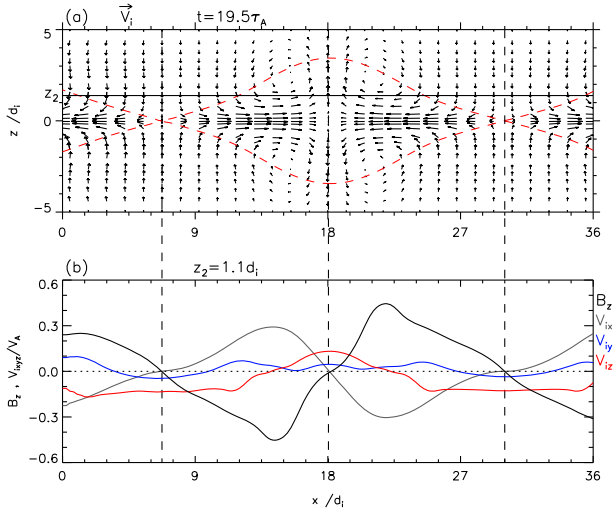

Figure 5. Panel a is the velocity vector of the plasma flow (arrows) and the magnetic separatrices (red dashed line) for Case 3 at $t = 19.5\tau_A$. B_z, V_{ix}, V_{iy}, and V_{iz} along the cut line are plotted in panel b. The vertical dashed lines denote the B_z-reversal points.

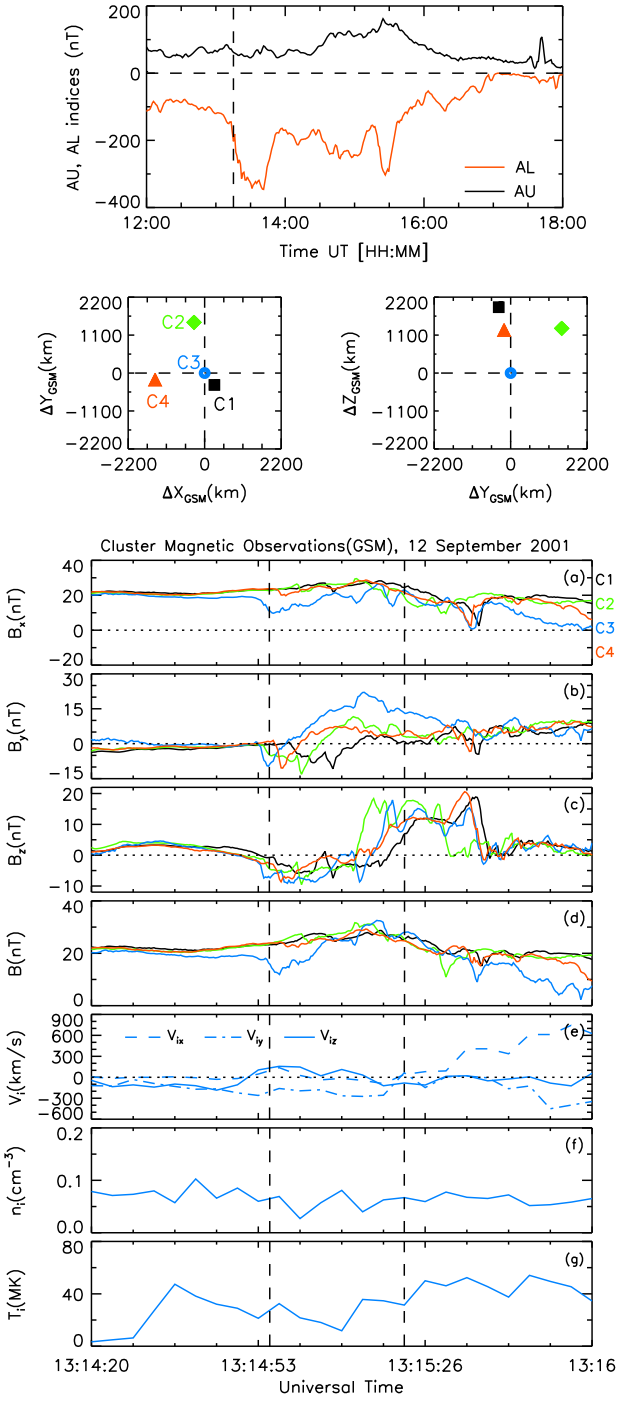

Figure 6. The top panel show the *AU* and *AL* geomagnetic indices during 12:00–18:00 UT on 12 September 2001, in which the vertical dashed line at 13:15 UT indicates the time of the plasmoid-2 event. The middle two panels display the relative position of the four Cluster satellites in the *XY* plane (left) and *YZ* plane (right), in GSM coordinates. Figure 6a–6g give a overview of Cluster data for 12 September 2001, 13:14:20–13:16:00 UT, in which the two vertical dashed lines delimit the time interval 10:08:33–10:08:44 UT that we used to reconstruct the plasmoid-2 using Cluster-3 data (blue line).

positions of four Cluster satellites at 13:15:06 UT. The position of Cluster 3 ($X_{GSM} \sim -18.8R_E$, $Y_{GSM} \sim 3.1R_E$, and $Z_{GSM} \sim 1.2R_E$) was selected as the initial reference point. The maximum separation distance between the four Cluster was ~ 2000 km in the *Z*-GSM direction, indicating that plasmoid-2 has a spatial scale on the order of 2000 km in the *z*-direction at least. Plasmoid-2 was first observed by Cluster 4, and then the theoretical order of spacecraft based on the *x*-coordinates (see left *XY* panel) is Cluster 2, 3, and 1. Figures 6a–6g show an overview of magnetic field and plasma parameter data obtained by Cluster spacecraft for the interval from 13:14:20 UT to 13:16:00 UT on 12 September 2001. We show here only the data from Cluster 3 in Figures 6e–6g. Here, we will apply single spacecraft [*Hu and Sonnerup*, 2002] GS reconstruction method to the Cluster 3 observations for recovery of two-dimensional magnetohydrostatic structures of plasmoid-2. The interval (13:14:54–13:15:24 UT) used for GS technique is bounded by the two vertical dashed lines. The GS method [*Hau and Sonnerup*, 1999] uses several assumptions that (1) the structure observed to be reconstructed have a magnetohydrodynamics (MHD) steady-state equilibrium: $\nabla p = \mathbf{j} \times \mathbf{B}$; (2) the spatial variation along the invariant *z*-axis changes much more gently (i.e., $\partial/\partial z \approx 0$) in comparison to the variations on the transverse cross section perpendicular to it; (3) the data analyzed here is based on the deHoffmann-Teller (HT) frame [*deHoffmann and Teller*, 1950] of reference, in which the convection electric field vanishes. Here, the 2.5-D magnetic structure is reconstructed in the *xy* plane and the invariant axis is along the *z* direction. The magnetic field vector is given by: $\mathbf{B} = [\partial A/\partial y, -\partial A/\partial x, B_z(A)]$, where $A(x,y)\hat{z}$ is the magnetic vector potential. Under the above conditions, the GS equation has the following form:

$$\left(\frac{\partial^2}{\partial x^2} + \frac{\partial^2}{\partial y^2}\right) A = -\mu_0 \frac{d}{dA}\left(p + \frac{B_z^2}{2\mu_0}\right), \qquad (1)$$

where the plasma pressure p, the axial magnetic pressure $B_z^2/2\mu_0$, and the transverse pressure $P_t = p + B_z^2/2\mu_0$ are the functions of A alone. The spatial initial values using a single satellite observations, the GS equation (1) can be solved numerically using the Taylor expansions (2) and (3) in a rectangular region (within the *xy* plane) to get the 2-D distribution of A.

$$A(x, y \pm \Delta y) \approx A(x,y) + \left(\frac{\partial A}{\partial y}\right)_{x,y} (\pm\Delta y) + \frac{1}{2}\left(\frac{\partial^2 A}{\partial y^2}\right)_{x,y} (\pm\Delta y)^2, \qquad (2)$$

$$B_x(x, y \pm \Delta y) \approx B_x(x,y) + \left(\frac{\partial^2 A}{\partial y^2}\right)_{x,y} (\pm\Delta y). \qquad (3)$$

Here, the GS equation is solved using the GS magnetic field reconstruction code [*Möstl et al.*, 2009]. The minimum variance analysis (MVA) method has been used to search for the initial frame $(\hat{x}', \hat{y}', \hat{z}')$ where the minimum variance direction $\hat{z}'$ is taken as the first approximation to the invariant axis of plasmoid-2. The initial coordinate system is: $\hat{x}' = [-0.025, -0.635, -0.771], \hat{y}' = [0.011, 0.771, -0.635], \hat{z}' = [0.999, -0.024, -0.012]$ (the flux rope axis) in GSM, with the eigenvalues of 446.404, 153.279, and –51,239.7, respectively. In order to find out the invariant axis, we continuously carried out $\hat{z}'$ axis rotation on each step by calculating the scatter for plot of $P_t(A)$ versus A in each experimental direction. The orientation associated with the minimum scatter is

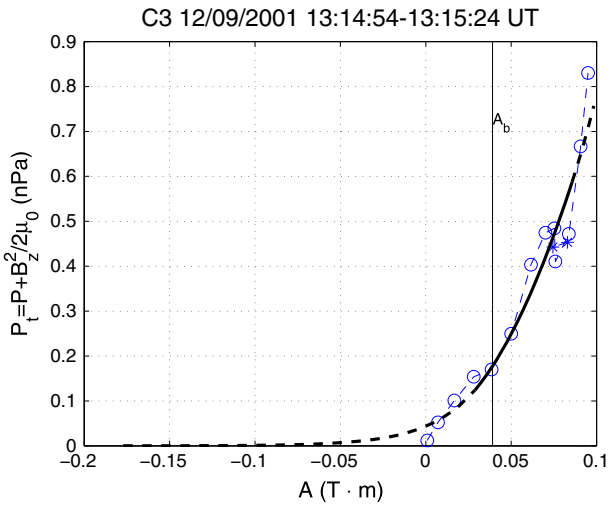

Figure 7. Plot of the observed transverse pressure P_t versus the computed partial vector potential A and its fitted curve for Cluster 3.

considered to be the invariant axis of plasmoid-2. Figure 7 shows the plot of $P_t(A)$, which was fitted by a second-order polynomial. Low residue of $R_f = 0.06$ is found. The $P_t(A)$ function is close to being single-valued, which is divided by a vertical black line at A_b. All these results indicate the reconstruction of plasmoid-2 is reliable. The boundary A_b is marked by the thick white contour in the map of the magnetic field (Figure 8) and notes where the single-valuedness of $P_t(A)$ lost. Figure 8 shows the contours of $A(x,y)$ and $B_z(A)$, where the black contour lines represent A, and the color is the magnetic field $B_z(A)$ distribution in the transverse plane perpendicular to the invariant axis. The magnetic field (in gray) and velocity (in black) components recorded along the Cluster spacecraft 3 trajectory are displayed as arrows, projected into the reconstruction plane. The GS reconstruction shows that a flux-rope-like plasmoid was moving tailward. Generally speaking, the two ends of the flux rope are connected to the Earth. Sometimes, the whole flux rope is dragged into a slingshot shaped during convection toward Earth or tail. In this case, the axial direction of the curved part of flux rope may be parallel to the x-axis. A cross-sectional view of the flux rope reconstructed by GS is an oval rather than circular in shape when the satellite crosses this type of flux rope. The observations of plasmoid-2 may be similar to the above-described spatial configuration.

3. Hall MHD Simulations

[19] The mechanism for the formation of plasmoid in the magnetotail can be understood as multiple X-line reconnection, which had been used to explain the FTEs formation by *Lee et al.* [1985]. In the following, we reproduce the observed features of small-scale plasmoids using Hall-MHD simulation. The possible formation mechanism of these observations will be discussed. Multiple X-lines reconnection within a long thin current sheet is triggered by the driven plasma inflow in simulations, which is prone to producing plasmoid between two adjacent reconnection points. The moving plasmoids are studied under different conditions for initial guide field (i.e., B_{y0}). By comparison, the simulation results can well reproduce the observed features of the typical plasmoid.

3.1. Simulation Model

[20] Simulations were run in a right-handed Cartesian (x,z) coordinate system where the positive x-axis direction is tailward, the positive z-axis points northward, and the y-axis is perpendicular to the xz-plane. In the two-dimensional case with the independent variable z, we may introduce a magnetic flux function $A(x,z,t)$ given by

$$\mathbf{B} = \nabla \times (A\mathbf{e}_y) + B_y\mathbf{e}_y. \tag{4}$$

The simulations start with a Harris current sheet equilibrium [*Harris*, 1962]. This initial magnetic field configuration can be expressed as

$$B_x(x,z) = -B_0 \tanh(z/L_c), \quad B_z(x,z) = 0, \tag{5}$$

and the corresponding magnetic flux function is

$$A(x,z) = A_0 \ln(\cosh(z/L_c)), \tag{6}$$

where B_0 is the initial value of B_x field at the top and bottom boundaries and L_c is the half-width of the initial current sheet. In order to facilitate the multiple X-line reconnection, L_c was set to be $L_c = 0.04L_0$, where L_0 is the half length of simulation box in z direction. The static isothermal equilibrium state is chosen as $V_x(x,z) = V_y(x,z) = V_z(x,z) = 0$, $T(x,z) = T_0$, and $\rho(x,z) = \rho_0 + \rho_c \mathrm{sech}^2(z/L_c)$, and ρ_c is determined by $RT_0\rho_c = B_0^2/8\pi$ (R is the gas constant) and

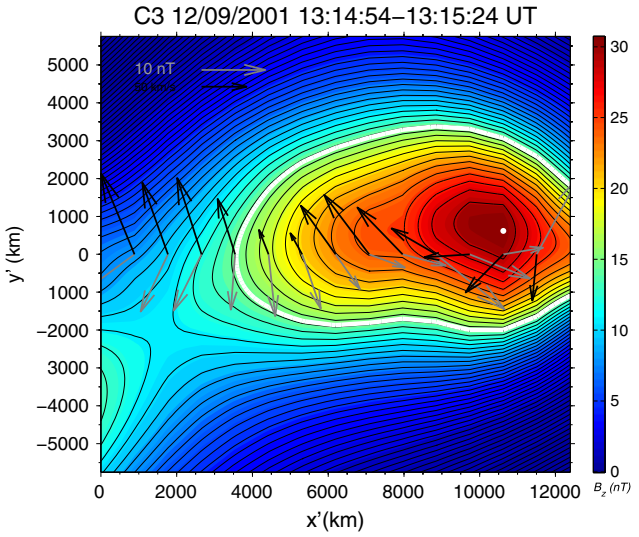

Figure 8. The reconstructed magnetic field map from Cluster 3 observations for the interval 10:08:33–10:08:44 UT. The black contour lines are the transverse (x'-y' plane) magnetic field lines, and the color contour shows the intensity of the axial (z') magnetic field B_z with its maximum marked by the white dot. In the figure, the gray arrows are measured magnetic field vectors projected onto the x'-y' plane along the spacecraft trajectory, and the black arrows are measured transverse velocities transformed into the HT frame.

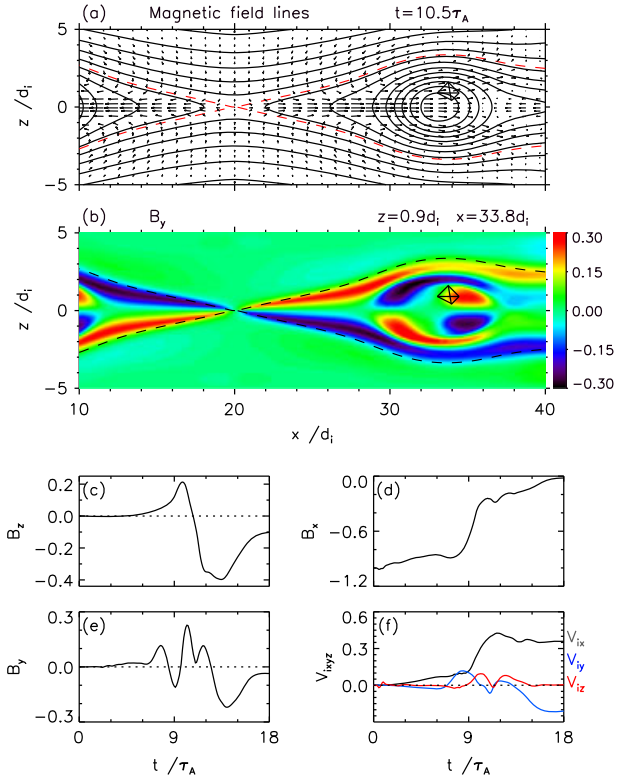

Figure 9. (a) The magnetic field line (solid line) and the velocity vector of the plasma flow (arrows), (b) contours of our-of-plane magnetic field B_y (color plot) for Case 1 with $B_{y0} = 0$ at $t = 10.5\tau_A$, and c to f time variations of B_z, B_x, B_y V_{ix}, V_{iy}, and V_{iz} at the given point $x = 33.8d_i$, $z = 0.9d_i$ (see panels a and b marked by tetrahedral symbol).

$\rho_c = 2.0\rho_0$. The initial equilibrium is not modified by the addition of a uniform out-of-plane magnetic field component B_{y0} [*Pritchett*, 2001], and in this way, the cases with the guide field $B_{y0} = 0$ and 0.5 (in unit of B_0) are investigated in this simulation.

[21] The 2.5-D Hall MHD equations are written in dimensionless forms as done by *Jin et al.* [2005] and *Yang et al.* [2006]. The length, magnetic field strength, density, temperature, magnetic flux function, velocity, and time are scaled by L_0, B_0, ρ_0, T_0, $A_0 = B_0L_0$, $V_A = B_0/\sqrt{\rho_0}$, and $\tau_A = L_0/V_A$, respectively. And the factor $(4\pi)^{1/2}$ is absorbed in the unit of B_0, so that $1/4\pi$ does not appear in Lorentz force terms. The dimensionless parameters χ_m, K_H, and K_P are given by

$$\chi_m = \frac{\eta}{V_A L_0},\ K_H = \frac{d_i}{L_0},\ K_P = \frac{\beta}{2}\frac{d_i}{L_0}, \tag{7}$$

where η is the plasma resistivity and $\beta = P_0/(B_0^2/2)$ is the ratio of plasma pressure to magnetic pressure outside the current sheet. In the present study, the resistivity η is assumed to be uniform, and the Lundquist number S (= $L_0V_A/\eta = 1/\chi_m$) is set as 2500. The other parameters are taken as follows: $T_0 = 6.48 \times 10^7$K, $B_0 = 30$nT, $\rho_0 = 1.67 \times 10^{-25}$g/cm^3 (corresponding to $n_{\rm ion} = 0.1$ protons/cm^3), $d_i = c/\omega_{pi} = c/\sqrt{\frac{4\pi e^2 n_0}{m_i}} = 720$ km, $L_0 = 5d_i$, and $\beta = 0.5$.

[22] The numerical simulations are carried out in a rectangular region defined by $0 \le L_x \le 8L_0$, $-L_0 \le L_z \le L_0$. Along the left boundary ($x = 0$) and right boundary ($x = L_x = 8$), ρ, V_x, V_y, V_z, B_y, and T are determined by linear extrapolation. We set $\partial^2 A/\partial x^2 = 0$ (i.e., $\partial B_z/\partial x = 0$) at the left and right boundaries. Along the top boundary ($z = L_0$) and bottom boundary ($z = -L_0$), the parameters ρ, T, B_y, V_x, and V_y are fixed, and $\partial^2 A/\partial z\partial t$ is set to be zero (i.e., $\partial B_x/\partial t = 0$). In order to simulate the situation of the multiple X-line reconnection, in which the moving plasmoids is involved, the inflows V_z (in unit of V_A) imposed at the top and bottom boundaries are assumed to be the following properties: At $x = L_x/2$, the maximum inflows are $V_z = \mp(V_1 + V_2)$, and then gradually decrease to $\mp V_1$ at $x = L_x/2 \pm L_x/16$. In the regions from $x = L_x/2 - L_x/16$ to $x = L_x/2 + L_x/16$, the inflows $\mp V_z$ are expressed as:

$$|V_z| = V_2[1 \mp \cos((8x/L_x - 7/2)\pi)] + V_1, \tag{8}$$

where the negative and positive signs correspond to the regions $7L_x/16 < x \le Ł_x/2$ and $L_x/2 \le x < 9L_x/16$, respec-

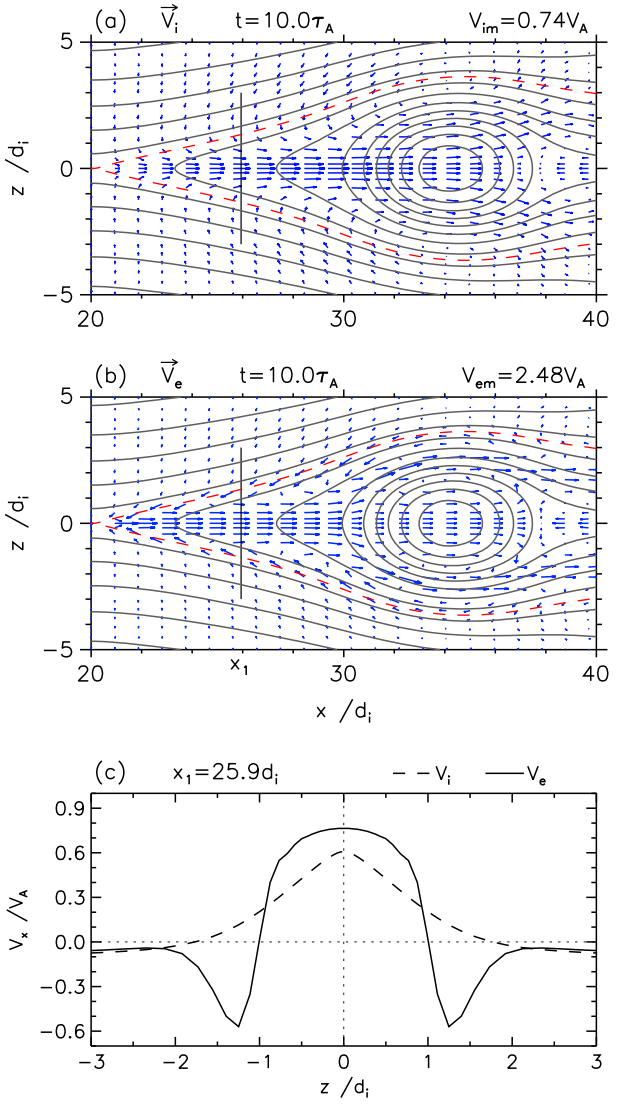

Figure 10. At $t = 10.0\tau_A$, the velocity vector plots of (a) ion flow and (b) electron flow in the (x,z) plane, and (c) the profiles of the V_x components in the ion (dashed line) and electron (solid line) flows along z at $x_1 = 25.9d_i$ for Case 1.

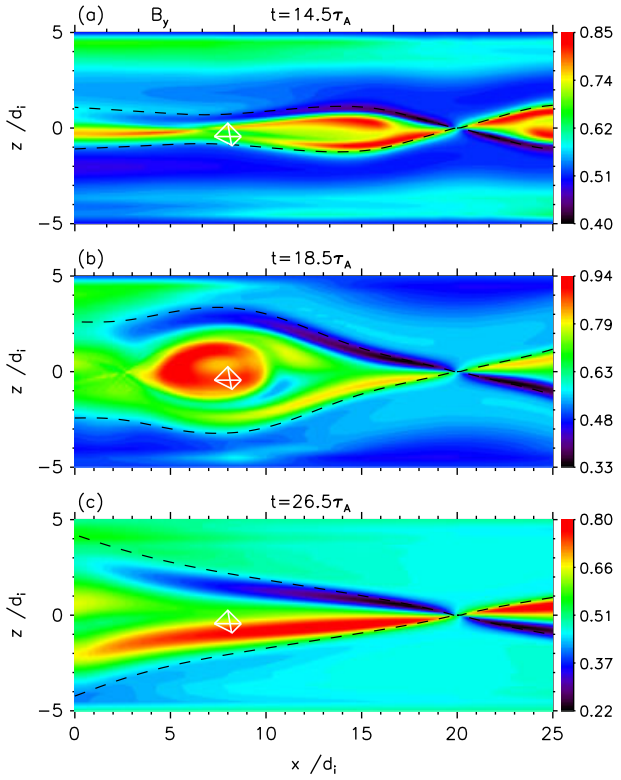

Figure 11. Time evolution of the contour maps of out-of-plane magnetic field B_y for Case 2 with $B_{y0} = 0.5$ at (a) $t = 14.5\tau_A$, (b) $t = 18.5\tau_A$, and (c) $t = 26.5\tau_A$.

tively. V_z are maintained at $\mp V_1$ in the ranges of $2L_x/16 \leq x \leq 7L_x/16$ and $9L_x/16 \leq x \leq 14L_x/16$. The inflows V_z are reduced to 0 from $2L_x/16$ and $14L_x/16$ to the left and right ends ($x = 0$ and $x = L_x$) of the top and bottom boundaries in terms of a cosine pattern. Here, $V_1 = 0.055$ and $V_2 = 0.09$ (in unit of V_A).

[23] The 2.5-D MHD equations are solved by a Hall MHD code [*Yang and Jin*, 2004] derived from multistep implicit scheme [*Hu*, 1989]. The computational domain is divided into 241 × 61 grid points. In order to get sufficient spatial resolution in the current sheet, the grid spacing in the z direction from $z = 0$ to $z = \pm L_0$ increases according to a geometric series. In the x direction, the computation from $x = 0$ to $x = 8L_0$ is advanced by a uniform grid-point spacing $\triangle x = 0.05$. To ensure computational accuracy and numerical stability, the time steps $\triangle t$ are required to satisfy the following Courant condition: $\triangle t \leq \triangle L/V_{max}$, where $\triangle L$ is the minimum grid spacing and V_{max} is the maximum velocity in the simulation box.

3.2. Simulation Results for Case 1 With Zero Guide Field

[24] In Case 1 with no guide field (i.e., $B_{y0} = 0$), the initial static equilibrium is broken by the inflows with the pattern mentioned above imposed at the top and bottom boundaries. Consequently the multiple X-line reconnection occurs in the long current sheet. The reconnection rate for each of these reconnection points can be different [*Schindler*, 1974]. The plasmoid bounded between the two X lines is embedded in bursty bulk outflows. Subsequently, it is swept away from the fastest reconnection site.

[25] Figure 9 summarizes the simulation results for Case 1. At $t = 10.5\tau_A$, the magnetic field and ion velocity distribution in the xy plane are plotted in panels (a) and (b). To clearly illustrate the distribution of ion velocity in plasmoid, only the data ranges from $10d_i$ to $40d_i$ in the x-axis direction are displayed in Figure 9a, where the magnetic field lines, plasma flow vectors, and magnetic separatrice are shown by the solid lines, arrows, and dashed lines, respectively. In Figure 9a, a tailward-moving plasmoid is separated by two neighboring reconnection x-points. These two reconnection points have different reconnection rates. Driven by the continuous inflow, the fastest reconnection occurs at standing site $x = 20d_i, z = 0d_i$. However, the second reconnection point with reconnection subrate is at right and moving toward the tail along the current sheet. The plasmoid is ejected sideways due to the magnetic field tension force and outflow jet. Figure 9b shows the magnetic field B_y with ± 0.3 around the reconnection X point ($x = 20d_i$, $z = 0d_i$). The quadrupolar magnetic field B_y with reversal polar related to neighboring reconnection sites is shown in the plasmoid.

[26] In order to display the development of the magnetic field and plasma velocity within the plasmoid, we selected a standing point $z = 0.9d_i, x = 33.8d_i$ (see Figures 9a and 9b denoted by tetrahedron). B_z, B_x, B_y, V_{ix}, V_{iy}, and V_{iz}

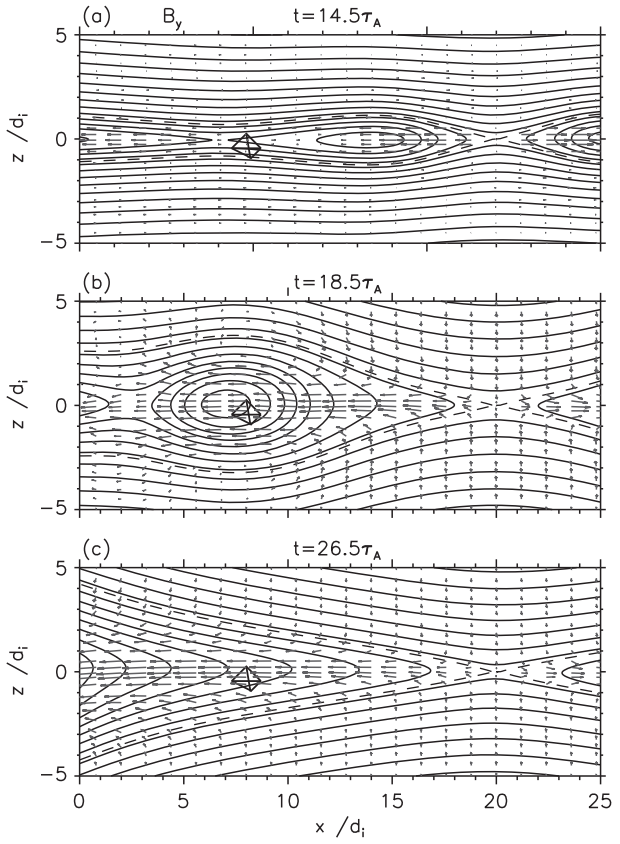

Figure 12. Time evolution of the magnetic field line (solid line) and the velocity vector of the plasma flow (arrows) for Case 2 with $B_{y0} = 0.5$ at (a) $t = 14.5\tau_A$, (b) $t = 18.5\tau_A$, and (c) $t = 26.5\tau_A$.

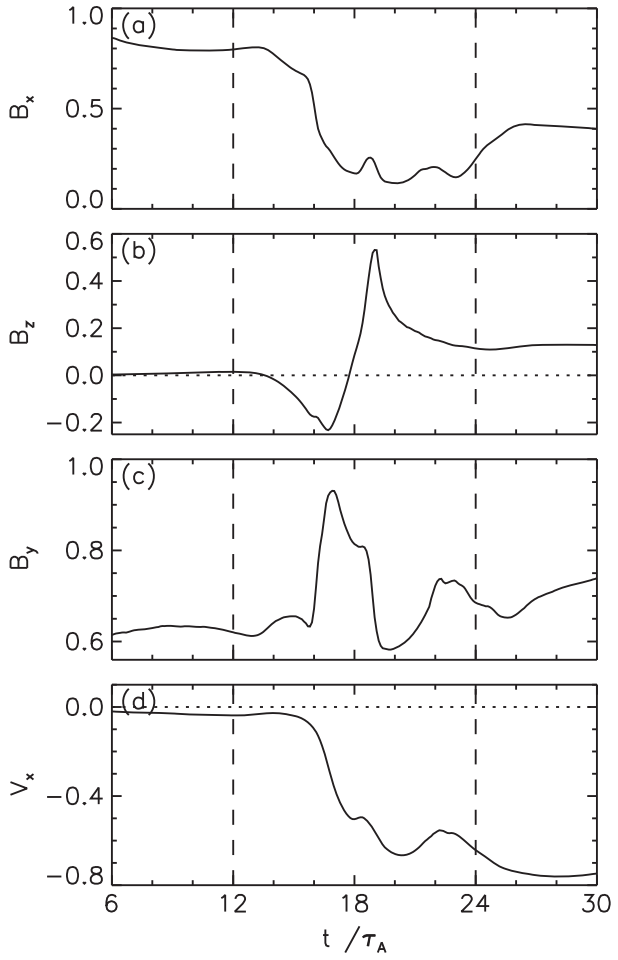

Figure 13. Time variations of B_x, B_z, B_y and V_x for Case 2 at given point $x = 33.8d_i, z = 0.9d_i$ (see Figures 11 and 12 marked by tetrahedral symbol).

were recorded (see Figures 9c–9f). Here, the selected point is close to the center of the plasmoid. V_{ix} increases slowly at first ($0 \sim 9\tau_A$), and them rapidly. V_{iy} and V_{iz} are close to zero. Within the plasmoid, $|V_{ix}|_{\max}/|V_{iy}|_{\max}$, $|V_{ix}|_{\max}/|V_{iz}|_{\max}$ are 3.6 and 4.5, respectively. The results are qualitatively similar to the observations (as seen Figures 2f–2h). During the moving plasmoid passes through the selected point, the multiple bipolar (also called "waveform") B_y signature associated with the bipolar (+/–) B_z signature is recorded. The value of B_x reaches the minimum at the center of plasmoid. Such signatures of B_x, B_y, and B_z recorded above are qualitatively comparable with the observations.

[27] The distributions of the ion velocity $\mathbf{V}_i$ and electron velocity $\mathbf{V}_e \approx \mathbf{V}_i - K_H\mathbf{J}/n$ at $t = 10\tau_A$ are shown in Figures 10a and 10b. Here, the only simulation zone $20d_i \le x \le 40d_i$ are plotted. The velocity vectors of plasma flow, magnetic field lines, and magnetic separatrices are expressed by the blue arrows, solid lines, and red dashed lines, respectively. As seen in Figures 10a and 10b, the maximum speed of the ion flow ($V_i|_{\max} = 0.74V_A$) is much less than that of electron flow ($V_e|_{\max} = 2.48V_A$). In particular, the speed of the electron flow is much faster than the ion flow around the X line, and the moving directions of the electron flow is more complex compared to the ion flow near the separatrices and in the plasmoid. To better illustrate the difference between the ion and electron flow, a cut line have been done at $x_1 = 25.9d_i$ along the z direction (see Figures 10a and 10b). The x component of the ion velocity and electron velocity along these cut lines are plotted in Figure 10c where V_i and V_e are expressed by dashed and solid lines. Near the separatrices about at $z = \pm 1$, the direction of V_{ex} has changed its sign, implying there exist bidirectional electron flows therein: one moves toward the x line and another moves away from the x line. However, at the same time, the direction of the ion flow have always keep positive signature, and the value of the ion flow is much less than the electron flow. Within the reconnection outflow zone about between $-1d_i$ and $1d_i$, the electron flow is larger than the ion flow, and their directions keep the same. All these indicate that the decoupling between the electrons and ions have happened near the X line in the plasmoid [*Liu et al.*, 2009].

3.3. Simulation Results for Case 2 With Guide Field $B_{y0} = 0.5$

[28] In Case 2 with a guide field $B_{y0} = 0.5$, at three separate times ($t = 14.5, 18.5$ and $26.5\tau_A$), Figure 11 gives the contours of the magnetic field B_y and the magnetic separatrices by the color plots and the dashed lines. The plasmoid produced by multiple X-line reconnection is moving earthward. The contours of B_y in Figure 11 are significantly different from that in Figure 9b. As compared to Case 1, here follow two main difference. One is that B_y field has a unipolar structure and maintain a positive value at the X line, which caused by the superposition of the initial guide field $B_{y0} = 0.5$. However, as seen in Figure 9b, B_y field near the X line has a positive and negative quadrupolar structure. Another one is that the strength of B_y in the plasmoid is nearly uniform growth at first until $t = 14.5\tau_A$, and then increased rapidly (Figure 11a). At last, the position of the maximum B_y moves into the plasmoid center. In Figure 11b, the plasmoid with enhanced out-of-plane field B_y moves earthward. The B_y flux is constantly convected from the lobe regions to the central part of plasmoid by magnetic reconnection, which causes enhancement of the core field in plasmoid.

[29] At three times $t = 14.5, 18.5, 26.5\tau_A$, Figure 12 shows the evolution of the magnetic field lines and velocity vectors of plasma flows by the solid lines and arrows. As seen in Figure 12a, a prolate plasmoid emerges in the current sheet. There are two reconnection X lines on its sides. The maximum ion velocity can be found near the right reconnection X line as shown by the scaled arrow length. This indicates that the maximum reconnection rate is located on the right X-point. As the magnetic reconnection proceeds, the plasmoid gradually grows in size, as it travels to earthward, which is also embedded in high-speed reconnection outflow region (Figure 12b). The plasmoid is pushed to move earthward by the high-speed outflow from the right X line, and departs from the simulation domain at $t = 26.5\tau_A$. Finally, Figure 12c presents a quasi-steady single X-line reconnection site at the central point ($x = 20d_i, z = 0d_i$) of the simulation domain.

[30] To better explore the moving plasmoid's structure, in Figure13, we have plotted the time evolution of B_x, B_y, B_z, and V_x at the given point ($x = 8.0d_i, z = -0.45d_i$) in

the center of the tetrahedron (see Figures 11 and 12). In Figure 13, the time windows delimited by the two vertical dashed lines in all panels approximately indicate the time interval ($12\tau_A \sim 24\tau_A$) during which the moving plasmoid passes through the given point. In Figure 13b, the history of B_z exhibits the bipolar negative/positive signature, implying that an earthward traveling plasmoid was recorded. The intensity of B_x in the central region of plasmoid is small compared to its surroundings. In Figure 13c, the strength of B_y is significantly increased at the plasmoid center. Such a significant enhancement of B_y might be representative of the observed strong core field of flux rope [*Liu et al.*, 2009]. At the given point, the time development of V_x (in unit of the Alfvén speed V_A) is shown in Figure 13d. The earthward flow enhancement sharp speed increase up to $0.65V_A$ at $19\tau_A$. It indicates that the earthward high-speed flow within the current sheet from the reconnection X-point exists inside the plasmoid. After the plasmoid moved out of the given point (after about $24\tau_A$), the amplitude of V_x always remains at $0.8V_A$, which corresponds to the continued occurrence of the single X-line reconnection at the center point of the simulation box (Figure 12c).

4. Summary and Conclusions

[31] In this paper, using data from Cluster spacecraft, we have presented a detailed analysis of the observations for several plasmoids in the magnetotail, and some of them are reported for the first time by us. The observation survey is divided into two types. The first one is the isolated plasmoid with two typical plasmoid events. The second type contains multiple successive plasmoids during a substorm. Especially for the second plasmoid, three main features were observed, including a core field in the plasmoid, a quadrupole magnetic field near the X line, and a local plasma convection within the plasmoid. The Grad-Shafranov reconstruction method was used to recover the two-dimensional magnetic field maps for plasmoid-2. These results may provide evidence that the small-scale plasmoid frequently observed in the magnetotail may be produced by multiple X-line collisionless reconnection. In general, the plasmoid has the following observed magnetic field properties: (1) The time series of magnetic data exhibit a bipolar B_z signature. The bipolar B_z variation with a north-to-south reversal or vice versa is associated with the directions of traveling plasmoids (earthward or tailward). (2) Associated with the bipolar B_z signature, often a very large core B_y magnetic field along the crosstail direction is observed, which indicates that there exists a closed magnetic field lines wrapping around the flux-rope-like core structure. (3) Within the plasmoid, the strength of ambient magnetic field B_x decreases closely to zero, and the profile of B_x has a pulse-type bulge processes relative to its background values. The existence of a bipolar signature in B_z followed by BBF. The overall structure of plasmoid is embedded in a bulk flow.

[32] To present the observational features of plasmoid, two simulation cases were performed: In Case 1, we chose $B_{y0} = 0$ to investigate the structures of plasmoid with a closed magnetic loop type. Case 2 was run with $B_{y0} = 0.5$ to simulate the observation structures of plasmoid with a flux-rope type. Case 2 corresponds to a situation that there exists a finite crosstail magnetic field component B_y in magnetotail. The 2.5-D Hall MHD simulation results are presented in section 3 for both cases. The results shows that the small part of the active thin and long current sheet is associated with magnetotail reconnection. In order to better compare the simulation results with the observations, the plasma parameter settings in the simulations could be compared with the plasma environment in the magnetotail. The driven inflow was imposed on the top and bottom boundaries, under the assumption of the existence of a dawn-to-dusk crosstail electric field in the magnetotail lobes. The multiple X-line reconnection has been triggered in the current sheet. The formation of plasmoids between pairs of active reconnection sites is a natural result of the multiple X-line reconnection, which was originally used to explain the structures of FTEs [*Lee et al.*, 1985]. Likewise, because of a preexisting crosstail component B_y in the magnetotail, a structure with enhanced core magnetic as a flux-rope-like would be formed in plasmoid [*Hughes and Sibeck*, 1987]. We compare the results of two simulation cases with the observations to analyze the typical characteristics of plasmoid. The quantitative comparisons show that these characteristics of the observations are in good agreement with the simulation results.

[33] The plasmoid observed in the magnetotail region [*Slavin et al.*, 2003a] have a scale length $< 5R_E$ much smaller than those with a large scale found in the distant magnetotail [*Slavin et al.*, 1995]. It is noteworthy that the spatial characteristic scale of these plasmoids are significantly smaller than those observed in the distant magnetotail. Also note that these plasmoids often closely associated with BBF, reaching its peak within roughly $1 \sim 2$ minute. The continued high-speed flow after the plasmoids encounter suggests that the reconnection is still active at X line.

[34] A large core field B_y is often observed near the center region of most plasmoids, whose maximum even can exceeds the ambient lobe field strength, and their directions and strengths are highly correlated with the IMF B_y strength and direction [*Hughes and Sibeck*, 1987]. This study shows that the direction of the core field B_y of the flux-rope-like plasmoids is in the same direction as the IMF B_y component. In general, we found that the preexisting crosstail magnetic field for about 2 h preceding the plasmoid event can cause more flux-rope-like plasmoids compared with closed-loop-like plasmoids. However, sometimes the profiles of B_y field in the plasmoid shows a bipolar or multiple bipolar signals (here we simply call it "wave," compared to the "core" statement) rather than a unipolar peak signal. The generation mechanism of these multiple bipolar signals may be associated with the Hall effects within the plasmoids as shown in Figure 9.

[35] The relationship between plasmoid and substorm has been extensively surveyed [*Slavin et al.*, 1992; *Moldwin and Hughes*, 1993; *Nagai et al.*, 1994; *Tang et al.*, 2009]. Observations showed that there exists a thin and elongated current sheet in substorms [*Sergeev et al.*, 1993], which may be regarded as part of the evolution of the magnetotail. Tearing mode instability [*Schindler*, 1974] often occurs in the thinned crosstail current layer, and their development can leads to spontaneous formation of the multiple plasmoids in the magnetotail region. Of course the reconnection can also be driven via external conditions. Sometimes, the thickness of the current sheet reaches the order of a fractions

of R_E before the substorm onset. When the thickness of the current sheet reaches the order of local ion gyro-radius, Hall effect can be considered as the important influencing factor for the formation of plasmoids structure. This situation is also shown in our observations and simulations.

[36] The signals associated with plasmoids in the magnetotail, such as the out-of-plane quadrupole magnetic field B_y around the X lines, the core field B_y in the plasmoid, are often reported individually. However, these two signals observed simultaneously have been rarely reported. Such results may be caused by the following several factors: (1) The spatial scale size of plasmoid is too small, resulting in a reduced chance of satellite observations. (2) The quadrupole field structure near the X lines may be covered due to the superposition effect of the preexisting crosstail field. (3) The existence of high-speed plasma streams associated with plasmoid can make some of the signals generated by the reconnection, such as the convective structures of plasma within the plasmoid, to be distorted and cannot easily be found. However, to further understand small-scale plasmoid structures requires frequent satellite observation and development of three-dimensional simulation. Further work of comparing these observations with three-dimensional Hall MHD simulation is in progress.

[37] **Acknowledgments.** This work is jointly supported by the National Basic Research Program of China under Grant 2012CB825601, the Knowledge Innovation Program of the Chinese Academy of Sciences (KZZD-EW-01-4), the National Natural Science Foundation of China (41231068, 41031066, 41204127, 41004082, and 41274192), and the Specialized Research Fund for State Key Laboratories. The *AL* and *AU* indices are provided by World Data Center for Geomagnetism, Kyoto. We thank the ACE MAG instrument teams and CDA Web for providing the solar wind data. We thank the Geotail/MGF instrument team for providing the magnetic field data used in this work. We would like to acknowledge the Cluster FGM and CIS instrument teams and the Cluster Active Archive (CAA) for the use of the Cluster data. We are especially grateful to Christian Möstl and Charles J. Farrugia, PhD, who provide a Grad-Shafranov reconstruction codes used in this study.

[38] Philippa Browning thanks James Slavin and another reviewer for their assistance in evaluating this paper.

References

Angelopoulos, V., W. Baumjohann, C. F. Kennel, F. V. Coroniti, M. G. Kivelson, R. Pellat, R. J. Walker, H. Lühr, and G. Paschmann (1992), Bursty bulk flows in the inner central plasma sheet, *J. Geophys. Res.*, *97*, 4027–4039.

Balogh, A., et al. (2001), The Cluster magnetic field investigation: Overview of inflight performance and initial results, *Ann. Geophys.*, *19*, 1207–1217.

Birn, J., J. F. Drake, M. A. Shay, B. N. Rogers, R. E. Denton, M. Hesse, M. Kuznetsova, Z. W. Ma, A. Bhattacharjee, A. Otto, and P. L. Prichett (2001), Geospace Environmental Modeling (GEM) magnetic reconnection challenge, *J. Geophys. Res.*, *106*, 3715.

Biskamp, D., E. Schwarz, and J. F. Drake (1997), Two-fluid theory of collisionless magnetic reconnection, *Phys. Plasmas*, *4*, 1002.

Borg, A. L., M. Øeroset, T. Phan, F. S. Mozer, A. Pedersen, C. Mouikis, J. P. McFadden, C. Twitty, A. Balogh, and H. Rème (2005), Cluster encounter of a magnetic reconnection diffusion region in the near-Earth magnetotail on September 19, 2003, *Geophys. Res. Lett.*, *32*, L19105, doi:10.1029/2005GL023794.

Chen, L. J., A. Bhattacharjee, P. A. Puhl-Quinn, H. Yang, N. Bessho, S. Imada, S. Mühlbachler, P. W. Daly, B. Lefebvre, Y. Khotyaintsev, A. Vaivads, A. Fazakerley, and E. Georgescu (2007), Observation of energetic electrons within magnetic islands, *Nature Phys. Lett.*, *4*, 19, doi: 10.1038/nphys777.

Cowley, S. W. H. (1981), Magnetospheric asymmetries associated with the *y*-component of the IMF, *Planet. Space Sci.*, *29*, 79–96.

Daughton, W., J. Scudder, and H. Karimabadi (2006), Fully kinetic simulations of undriven magnetic reconnection with open boundary conditions, *Phys. Plasmas*, *13*, 072101, doi:10.1063/1.2218817.

deHoffmann, F., and E. Teller (1950), Magnetohydrodynamic shocks, *Phys. Rev. A*, *80*, 692–703.

Deng, X. H., H. Matsumoto, H. Kojima, T. Mukai, R. R. Anderson, W. Baumjohann, and R. Nakamura (2004), Geotail encounter with reconnection diffusion region in the, Earth's magnetotail: Evidence of multiple X lines collisionless reconnection? *J. Geophys. Res.*, *109*, A05206, doi: 10.1029/2003JA010031.

Deng, X. H., and H. Matsumoto (2001), Rapid magnetic reconnection in the Earth's magnetosphere mediated by whistler waves, *Nature*, *410*, 557.

Drake, J. F., M. Swisdak, K. M. Schoeffler, B. N. Rogers, and S. Kobayashi (2006), Formation of secondary islands during magnetic reconnection, *Geophys. Res. Lett.*, *33*, L13105, doi:10.1029/2006GL025957.

Eastwood, J. P., D. G. Sibeck, J. A. Slavin, M. L. Goldstein, B. Lavraud, M. Sitnov, S. Imber, A. Balogh, E. A. Lucek, and I. Dandouras (2005), Observations of multiple X-line structure in the Earth's magnetotail current sheet: A Cluster case study, *Geophys. Res. Lett.*, *32*, L11105, doi: 10.1029/2005GL022509.

Eastwood, J. P., T.-D. Phan, F. S. Mozer, M. A. Shay, M. Fujimoto, A. Retinò, M. Hesse, A. Balogh, E. A. Lucek, and I. Dandouras (2007), Multi-point observations of the Hall electromagnetic field and secondary island formation during magnetic reconnection, *J. Geophys. Res.*, *112*, A06235, doi:10.1029/2006JA012158.

Eastwood, J. P., T. D. Phan, M Øieroset, and M. A. Shay (2010), Average properties of the magnetic reconnection ion diffusion region in the Earth's magnetotail: The 2001–2005 Cluster observations and comparison with simulations, *J. Geophys. Res.*, *115*, A08215, doi: 10.1029/2009JA014962.

Elphic, R. C., C. A. Cattell, K. Takahashi, S. J. Bame, and C. T. Russell (1986), ISEE-1 and 2 observations of magnetic flux ropes in the magnetotail: FTE's in the plasma sheet? *Geophys. Res. Lett.*, *13*, 648–651.

Fairfield, D. H. (1979), On the average configuration of the geomagnetic tail, *J. Geophys. Res.*, *84*(A5), 1950–1958.

Hall, E. H. (1879), On a new action of the magnet on electric currents, *Amer. J. Math.*, *2*(3), 287–292.

Hasegawa, H, R. Nakamura, M. Fujimoto, V. A. Sergeev, E. A. Lucek, H. Rème, and Y. Khotyaintsev (2007), Reconstruction of a bipolar magnetic signature in an earthward jet in the tail: Flux rope or 3D guide-field reconnection? *J. Geophys. Res.*, *112*, A11206, doi: 10.1029/2007JA012492.

Hau, L.-N., and B. U. Ö. Sonnerup (1999), Two-dimensional coherent structures in the magnetopause: Recovery of static equilibria from single-spacecraft data, *J. Geophys. Res.*, *104*, 6899–6917.

Henderson, P. D., C. J. Owen, I. V. Alexeev, J. Slavin, A. N. Fazakerley, E. Lucek, and H. Rème (2006), Cluster observations of flux rope structures in the near-tail, *Ann. Geophys.*, *24*, 651–666.

Hones, E. W. Jr (1976), The magnetotail: Its generation and dissipation, in *Physics of Solar Planetary Environments*, edited by D. J. Williams, pp. 559–571, AGU, Washington D. C.

Hones, E. W. Jr., D. N. Baker, S. M. Bame, W. C. Feldman, J. T. Gosling, D. J. McComas, R. D. Zwickl, J. A. Slavin, E. J. Smith, and B. T. Tsurutani (1984), Structure of the magnetotail at 220 R_E and its response to geomagnetic acivity, *Geophys. Res. Lett.*, *11*(1), 5–7.

Hu, Y. Q. (1989), A multistep implicit scheme for time-dependent two-dimensional magnetohydrodynamic flows, *J. Comput. Phys.*, *84* (10), 441–460.

Hu, Q., and B. U. Ö. Sonnerup (2002), Reconstruction of magnetic clouds in the solar wind: Orientations and configurations, *J. Geophys. Res.*, *107*(A7), 1142, doi:10.1029/2001JA000293.

Hughes, W. J., and D. G. Sibeck (1987), On the three-dimensional structure of plasmoids, *Geophy. Res. Lett.*, *14*(6), 636–639.

Ieda, A., S. Machida, T. Mukai, Y. Saito, T. Yamamoto, A. Nishida, T. Terasawa, and S. Kokubun (1998), Statistical analysis of the plasmoid evolution with Geotail observations, *J. Geohpys. Res.*, *103* (A3), 4453–4465.

Jin, S. P., H. A. Yang, and X. G. Wang (2005), Hall effect and fine structures in magnetic reconnection with high plasma β, *Phys. Plasmas*, *12*(4), 042902, doi:10.1063/1.1870003.

Karimabadi, H., D. Krauss-Varban, N. Omidi, and H. X. Vu (1999), Magnetic structure of the reconnection layer and core field generation in plasmoids, *J. Geophys. Res.*, *104*(A6), 12,313–12,326.

Kaufmann, R. L. (1987), Substorm currents: Growth phase and onset, *J. Geophys. Res.*, *92*(A7), 7471–7486.

Lee, L. C., Z. F. Fu, and S.-I. Akasofu (1985), A simulation study of forced reconnection processes and magnetospheric storms and substorms, *J. Geophys. Res.*, *90*, 10, 896–10,910.

Liu, C. X., S. P. Jin, and F. S. Wei (2011), Hall MHD simulations of collisionless multiple X line reconnection, *J. Geophys. Res.*, *116*, A03217, doi:10.1029/2010JA015992.

Liu, C. X., S. P. Jin, F. S. Wei, Q. M. Lu, and H. A. Yang (2009), Plasmoid-like structure in multiple X line Hall MHD reconnection, *J. Geophys. Res.*, *114*, A10208, doi:10.1029/2009JA014257.

Lui, A. T. Y. (1984), Characteristics of the cross-tail current in the Earth's magnetotail, in *Magnetospheric Currents, Geophys. Monogr. Ser.,* vol. 28, edited by T. A. Potemra, pp. 158–170, AGU, Washington, D.C.

Lui, A. T. Y., R. E. Lopez, B. J. Anderson, K. Takahashi, L. J. Zanetti, R. W. McEntire, T. A. Potemra, D. M. Klumpar, E. M. Greene, and R. Strangeway (1992), Current disruptions in the near-Earth neutral sheet region, *J. Geophys. Res.*, *97*(A2), 1461–1480.

Ma, Z. W., A. Otto, and L. C. Lee (1994), Core magnetic field enhancement in single, X line, multiple X line and patchy reconnection, *J. Geophys. Res.*, *99*, 6125–6136.

Moldwin, M. B., and W. J. Hughes (1991), Plasmoids as magnetic flux ropes, *J. Geohpys. Res.*, *96*(A8), 14,051–14,064.

Moldwin, M. B., and W. J. Hughes (1992), On the formation and evolution of plasmoids: A survey of ISEE 3 Geotail data, *J. Geohpys. Res.*, *97*(A12), 19,259–19,0282.

Moldwin, M. B., and W. J. Hughes (1993), Geomagnetic substorm association of plasmoids, *J. Geohpys. Res.*, *98*(A1), 81–88.

Möstl, C., C. J. Farrugia, C. Miklenic, M. Temmer, A. B. Galvin, J. G. Luhmann, E. K. J. Kilpua, M. Leitner, T. Nieves-Chinchilla, A. Veronig, and H. K. Biernat (2009), Multispacecraft recovery of a magnetic cloud and its origin from magnetic reconnection on the Sun, *J. Geophys. Res.*, *114*, A04102, doi:10.1029/2008JA013657.

Nagai, T., K. Takahashi, H. Kawano, T. Yamamoto, S. Kokubun, and A. Nishida (1994), Initial Geotail survey of magnetic substorm signatures in the magnetotail, *Geophys. Res. Lett.*, *21*, 2991–2994.

Ohtani, S., M. A. Shay, and T. Mukai (2004), Temporal structure of the fast convective flow in the plasma sheet: Comparison between observations and two-fluid simulations, *J. Geophys. Res.*, *109*, A03210, doi: 10.1029/2003JA010002.

Øieroset, M., T. D. Phan, M. Fujimoto, R. P. Lin, and R. P. Lepping (2001), In situ detection of collisionless reconnection in the Earth's magnetotail, *Nature*, *412*, 414.

Pritchett, P. L. (2001), Geospace Environmental Modeling magnetic reconnection challenge: Simulations with a full partical electromagnetic code, *J. Geophys. Res.*, *106*(A3), 3783.

Rème, H., et al. (2001), First multispacecraft ion measurements in and near the Earth's magnetosphere with the identical Cluster ion spectrometry (CIS) experiment, *Ann. Geophys.*, *19*, 1303–1354.

Ren, Y., M. Yamada, S. Gerhardt, H. Ji, R. Kulsrud, and A. Kuritsyn (2005), Experimental verification of the hall effect during magnetic reconnection in a laboratory plasma, *Phys. Rev. Lett.*, *95*(5), 005003.

Schindler, K. (1974), A theory of the substorm mechanism, *J. Geophys. Res.*, *79*(19), 2803–2810.

Sergeev, V. A., D. G. Mitchell, C. T. Russell, and D. J. Williams (1993), Structure of the tail plasma/current sheet at $\sim 11R_E$ and its changes in the course of a substorm, *J. Geophys. Res.*, *98*(A10), 17,345–17,365.

Shay, M. A., J. F. Drake, R. E. Denton, and D. Biskamp (1998), Structure of the dissaption region during collisionless magnetic reconnection, *J. Geophys. Res.*, *103*(A4), 9165.

Sibeck, D. G., G. L. Siscoe, J. A. Slavin, E. J. Smith, S. J. Bame, and F. L. Scarf (1984), Magnetotail flux ropes, *Geophys. Res. Lett.*, *11*(10), 1090–1093.

Slavin, J. A., C. J. Owen, M. M. Kuznetsova, and M. Hesse (1995), ISEE 3 observations of plasmoids with flux rope magnetic topologies, *Geophy. Res. Lett.*, *22*(15), 2061–2064.

Slavin, J. A., R. P. Lepping, J. Gjerloev, D. H. Fairfield, M. Hesse, C. J. Owen, M. B. Moldwin, T. Nagai, A. Ieda, and T. Mukai (2003a), Geotail observations of magnetic flux ropes in the plasma sheet, *J. Geophys. Res.*, *108*(A1), 1015, doi:10.1029/2002JA009557.

Slavin, J. A., R. P. Lepping, J. Gjerloev, D. H. Fairfield, M. Hesse, C. J. Owen, M. B. Moldwin, T. Nagai, A. Ieda, and T. Mukai (2003b), Cluster electric current density measurements within a magnetic flux rope in the plasma sheet, *Geophys. Res. Lett.*, *30* (7), 1362, doi: 10.1029/2002GL016411.

Slavin, J. A., et al. (1989), CDAW 8 observations of plasmoid signatures in the geomagnetic tail: An assessment, *J. Geophys. Res.*, *94*(A11), 15,153–15,175.

Slavin, J. A., M. F. Smith, E. L. Mazur, D. N. Baker, T. Iyemori, H. J. Singer, and E. W. Greenstadt (1992), ISEE 3 plamsoid and TCR observations during an extended interval of substorm activity, *Geophys. Res. Lett.*, *19*, 825–828.

Smith, C. W., J. L'Heureux, N. F. Ness, M. H. AcuÑa, L. F. Burlaga, and J. Scheifele (1998), The ACE magnetic fields experiment, *Space Sci. Rev.*, *86*, 613–632.

Sonnerup, B. U. Ö. (1979), Magnetic field reconnection, in *Solar System Plasma Physics,* vol. 3, edited by L. J. Lanzerotti, C. F. Kennel, and E. N. Parker, 46 pp., North Holland, New York.

Tang, C. L., Z. Y. Li, and L. Lu (2009), Cluster observations of earthward propagating plasmoid and flux ropes in the near-tail during the course of a substorm event, *Adv. Space Res.*, *43*, 1337–1342.

Terasawa, T. (1983), Hall current effect on tearing mode instability, *Geophys. Res. Lett.*, *10*(6), 475–478.

Vaivads, A., Y. Khotyaintsev, M. André, A. Retinò, S. C. Buchert, B. N. Rogers, P. Décréau, G. Paschmann, and T. D. Phan (2004), Structure of the magnetic reconnection diffusion region from four-spacecraft observations, *Phys. Rev. Lett.*, *93*(10), doi:10.1103/PhysRevLett.93.105001.

Walker, R. J., and T. Ogino (1996), A globle magnetohydrodynamic simulation of the origin and evolution of magnetic flux ropes in the magnetotail, *J. Geomagn. Geoelectr.*, *48*, 765–779.

Walsh, A. P., A. N. Fazakerley, R. J. Wilson, I. V. Alexeev, P. D. Henderson, C. J. Owen, E. Lucek, C. Carr, and I. Dandouras (2007), Near-simultaneous magnetotail flux rope observations with cluster and double star, *Ann. Geophys.*, *25*, 1887–1897.

Wang, R. S., Q. M. Lu, A. M. Du, and S. Wang (2010), In situ observations of a secondary magnetic island in an ion diffusion region and associated energetic electrons, *Phys. Rev. Lett.*, *104*, 175003, doi: 10.1103/PhysRevLett.104.175003.

Wang, X. G., A. Bhattacharjee, and Z. W. Ma (2001), Scaling of collisionless forced reconnection, *Phys. Rev. Lett.*, *87*(26), 265003.

Yang, H. A., S. P. Jin, and G. C. Zhou (2006), Density depletion and Hall effect in magnetic reconnection, *J. Geophys. Res*, *111*, A11223, doi: 10.1029/2005JA011536.

Yang, H. A., and S. P. Jin (2004), Effects of Hall current in the driven reconnection with various scales, *Chin. Phys. lett.*, *21*(7), 1394–1397.

Zong, Q.-G., et al. (1997), Geotail observations of energetic ion species and magnetic field in plasmoid-like structures in the course of an isolated substorm event, *J. Geophys. Res.*, *102*(A6), 11,409–11,428.

Zong, Q.-G., T. A. Fritz, Z. Y. Pu, S. Y. Fu, D. N. Baker, H. Zhang, A. T. Lui, I. Vogiatzis, K.-H. Glassmeier, A. Korth, P. W. Daly, A. Baloth, and H. Reme (2004), Cluster observations of earthward flowing plasmoid in the tail, *Geophys. Res. Lett.*, *31*, L18803, doi:10.1029/2004GL020692.